

The yttrium substitution impact on mechanical properties of biodegradable $\text{Mg}_{66}\text{Zn}_{30}\text{Ca}_4$ alloy

Zuzana Molčanová^{1*}, Beáta Ballóková¹, Wanda Miženková^{1,2}, Miroslav Džupon¹,
Dóra Zalka^{1,3}, Karel Saksal^{1,4}

¹*Institute of Materials Research, SAS, Watsonova 47, 040 01 Košice, Slovak Republic*

²*Faculty of Mechanical Engineering, Technical University of Košice, Letná 9, 042 00 Košice, Slovak Republic*

³*Faculty of Science, Pavol Jozef Šafárik University in Košice, Šrobárova 2, 041 80 Košice, Slovak Republic*

⁴*Faculty of Materials, Metallurgy and Recycling, Technical University of Košice, Letná 9, 042 00 Košice, Slovak Republic*

Received 16 September 2022, received in revised form 20 October 2022, accepted 20 October 2022

Abstract

From the point of view of possible medical applications, biodegradable alloys belong to hot-topic materials. Many different systems are studied in this field, seeking a compromise between mechanical-physical properties vs biocompatibility. Due to a suitable degradation rate, magnesium alloys, including zinc and iron, have been extensively investigated in recent years. The $\text{Mg}_{66}\text{Zn}_{30}\text{Ca}_4$ system is well known for its good mechanical properties and biocompatibility. In this work, we want to present a way how to improve the mechanical properties of this alloy by yttrium substitution. The $\text{Mg}_{66-x}\text{Zn}_{30}\text{Ca}_4\text{Y}_x$ ($x = 0, 2, 4, 6$) ingots were prepared by a rapid solidification process. The mechanical properties of modified alloys were compared with those of the starting alloy. Adding Y (up to 4 at.%) leads to an improvement of ultimate compressive strength. By Tafel plots, the prediction of corrosion rates of analyzed samples was estimated. A higher amount of Y (above 4 at.%) reduces corrosion.

Key words: biodegradable alloys, magnesium-based alloys, yttrium microalloying, compressive strength, corrosion resistance

1. Introduction

Conventional non-degradable biomaterials, such as stainless steel, cobalt-chromium alloys, titanium and its alloys, are used as permanent or temporary bone implants. These metallic materials have been used for diverse biomedical applications, e.g., joint replacement, fracture fixation, cardiovascular stents, and remodeling of bone, thanks to their high mechanical strength and corrosion resistance [1]. Impurities in these alloys (Al, V, Cr, and Ni) negatively affect their biocompatibility. The discrepancy between the human bone elastic modulus (15–30 GPa) [2] and that of above mentioned metallic materials (55–240 GPa) [3] leads to stresses and deformations of the surrounding bone tissue, bone resorption and implant loosening, which requires complex reoperation. In addition to corrosion-resistant biomaterials in medicine, great attention is paid to biodegradable materials.

For these new types of materials consisting only of elements that occur in the human body (biodegradable/bioresorbable), the reoperation problem is eliminated [4]. Biodegradable material gradually corrodes in the human body. The products of this process must not be toxic or carcinogenic and must therefore be easily eliminated from the body in natural ways. The main characteristics of such material can be summarized in two points: temporary support and degradation [5]. In addition, its decomposition products (Zn, Ca, and Mg ions) help heal and regenerate the surrounding damaged soft tissue. Biodegradable magnesium implants possess excellent mechanical properties and biocompatibility, making them suitable candidates to be employed as temporary structures for bone regeneration [6]. However, there are still important challenges that limit their extensive use in biomedical applications. The most important ones include implant-associated infection, rapid degradation

*Corresponding author: e-mail address: molcanova@saske.sk

rate, and the need for improved mechanical properties. This area aims to design alloys with good mechanical and corrosive properties and excellent biocompatibility. Studies in developing corrosion-resistant bioresorbable magnesium-based alloys suggest that by the suitable addition of microalloying, it is possible to increase their plastic deformability while maintaining excellent strength [7]. As mentioned above, magnesium and zinc alloys have emerged as one of the most promising materials in such research [8–10]. This potential arises mainly due to their reasonable degradation rate, which has been extensively investigated in recent years [11, 12]. As an experimental material for our research, the $\text{Mg}_{66}\text{Zn}_{30}\text{Ca}_4$ system was chosen. This alloy is well known for its good mechanical properties and biocompatibility [13, 14]. The main goal was to improve the mechanical and corrosion properties by microalloying with yttrium (Y). The positive effect of Y on the microstructure and hardness of various systems of Mg-based alloys was observed [15, 16]. In the case of Mg-Cu amorphous alloy, adding Y improved NaCl corrosion resistance [17].

2. Materials and methods

The experimental alloys $\text{Mg}_{66-x}\text{Zn}_{30}\text{Ca}_4\text{Y}_x$ ($x = 0, 2, 4, 6$ at.%) were prepared by induction melting in an inert atmosphere. The synthesis procedure was as follows: pure elements (Mg, Zn, Ca, and Y) were melted at 600°C in graphite crucibles in an induction furnace with an argon atmosphere. The melt was injected at 650°C into the water-cooled copper mold to produce alloy ingots. The final ingots were 130 mm in length and 3 mm in diameter. Microstructure and chemical composition were analyzed by scanning electron microscopy (SEM; TESCAN VEGA 3 LMU) equipped with an energy dispersive spectrometer (EDS). The phases in the alloys were identified by X-ray diffraction (XRD; Philips Xpert Pro) applying $\text{CuK}\alpha$ radiation. The samples for SEM observation were prepared by conventional metallographic procedure. The samples for compressive tests were cut out from cast samples into the shape of cylinders with 3 mm diameter and 6 mm length. The compressive tests were performed along the cast direction in a universal test machine TiraTest 2300. Nano-hardness and elastic modulus were tested by depth-sensing indentation (DSI) technique using a nano-indentation tester TTX-NHT; CSM Instruments with a Berkovich indenter (maximum load 150 mN, hold on 10 s, loading speed 300 mN min^{-1}). The obtained load-penetration depth ($P-h$) curves were treated according to Oliver and Pharr's analysis [18]. The values of hardness and elastic modulus as functions of depth, as well as elastic and plastic deformation energies, were calculated. The corrosion rate prediction was determined from polar-

Table 1. Chemical composition of the cast $\text{Mg}_{66-x}\text{Zn}_{30}\text{Ca}_4\text{Y}_x$ ($x = 0, 2, 4, 6$ at.%) alloys

Sample	Mg	Zn	Ca	Y
$\text{Mg}_{66}\text{Zn}_{30}\text{Ca}_4$	64	32	4	–
$\text{Mg}_{64}\text{Zn}_{30}\text{Ca}_4\text{Y}_2$	63	31	4	2
$\text{Mg}_{62}\text{Zn}_{30}\text{Ca}_4\text{Y}_4$	63	29	4	4
$\text{Mg}_{60}\text{Zn}_{30}\text{Ca}_4\text{Y}_6$	62	28	4	6

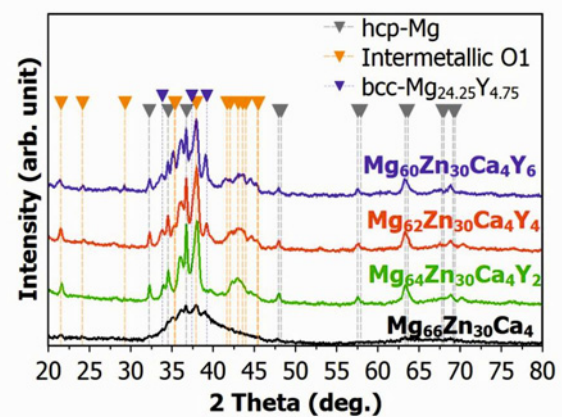


Fig. 1. X-ray diffraction patterns of the $\text{Mg}_{66-x}\text{Zn}_{30}\text{Ca}_4\text{Y}_x$ ($x = 0, 2, 4, 6$ at.%) alloys.

ization curves measured in Hank's solution at 33°C in a conventional three-electrode corrosion test cell where the alloy served as the working electrode, Pt was applied as the counter electrode, and Ag/AgCl electrode was the reference electrode. An Autolab VIONIC electrochemical working station was used controlled with the Intello software package for electrochemical measurements.

3. Results and discussion

3.1. Chemical composition

Table 1 shows the chemical composition of cast alloys. The detected composition of prepared cast ingots differed at level 2 at.% compared to the nominal composition for all samples.

3.2. Microstructure characterization

XRD patterns shown in Fig. 1 illustrate the rapidly solidified $\text{Mg}_{66-x}\text{Zn}_{30}\text{Ca}_4\text{Y}_x$ ($x = 0, 2, 4, 6$ at.%) alloys. The $\text{Mg}_{66}\text{Zn}_{30}\text{Ca}_4$ alloy has a dominant amorphous structure. As the Y fraction increases, the amorphous content gradually decreases, and sharp peaks

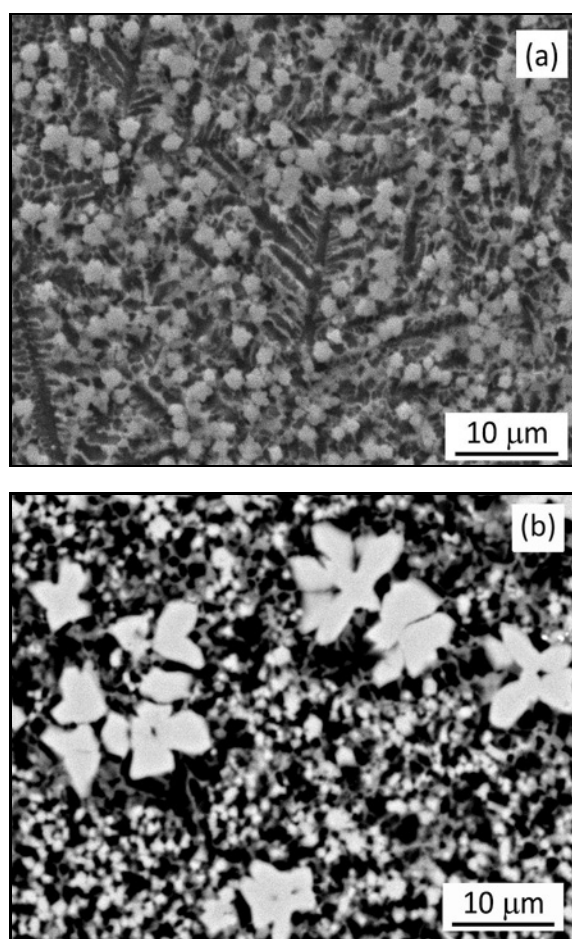


Fig. 2. SEM image of the Y_2 alloy (a) and Y_6 alloy (b).

appear. The alloys with Y addition contain three phases: α -Mg, $Mg_{24.25}Y_{4.75}$, and an unknown (labeled as O1) orthorhombic phase similar to the Ga_2Zr phase.

Figure 2 shows the SEM image of cast alloys. The $Mg_{66}Zn_{30}Ca_4$ alloy was homogeneous in the whole volume. By adding 2 at.% of Y (Fig. 2a), the dendritic structure and precipitated phase rich in Y were detected. With the further addition of Y to $Mg_{60}Zn_{30}Ca_4Y_6$, this Y-phase formed snowflake-like structures containing more than 20 at.% of Y (Fig. 2b). The Y-rich phase is most likely related to the unknown phase detected by X-ray.

3.3. Mechanical properties

Figure 3 shows compression strength curves of as-cast alloys. It can be seen that the ultimate compressive strength (UCS) and the plastic strain of doped alloys were significantly improved compared to alloys without Y. The UCS of the $Mg_{66}Zn_{30}Ca_4$ and $Mg_{64}Zn_{30}Ca_4Y_2$ alloys was 662 and 671 MPa, respectively. The highest UCS at 723 MPa was ob-

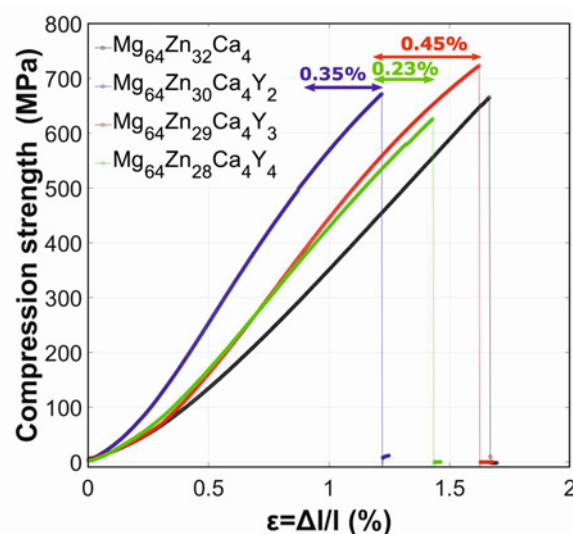


Fig. 3. The ultimate compressive strength of $Mg_{66-x}Zn_{30}Ca_4Y_x$ ($x = 0, 2, 4, 6$) ingots.

served for $Mg_{62}Zn_{30}Ca_4Y_4$ alloy. This alloy exhibits superior compressive ductility in comparison to the other alloys. The enhanced strength and plasticity of $Mg_{62}Zn_{30}Ca_4Y_4$ alloy may be attributed to the formation of the Y-rich phase in the matrix. This effect of improving the mechanical properties by yttrium alloying vanishes at 6 at.% of Y. The strength and plasticity are reduced as shown for $Mg_{60}Zn_{30}Ca_4Y_6$ alloy.

The fracture surface of all cast alloys is represented in Fig. 4. The SEM image indicates a typical brittle fracture. The stress passes through the Mg matrix during the compressive process, transferring the force to the Y-rich particles. Thus, the compressive stress of the $Mg_{66}Zn_{30}Ca_4$ BMG is remarkably improved due to the addition of Y. Additionally, the nano-hardness measurements were done, from which the hardness (H_{IT}) and elastic modulus (E_{IT}) were obtained. The H_{IT} values ranged from 3.22 ($Mg_{60}Zn_{30}Ca_4Y_6$) to 4 GPa ($Mg_{64}Zn_{30}Ca_4Y_2$). Elastic modulus increases with the Y-addition. While for the $Mg_{66}Zn_{30}Ca_4$ alloy it was 46 GPa, Y brings it to the range of 52 to 69 GPa. The sample density was approximately 3 g cm^{-3} . These values are very similar to the human bones, which makes them a potential candidate for medical implants.

The mechanical properties of as-cast alloys at room temperature are summarized in Table 2.

3.4. Corrosion properties

The corrosion rate was determined from the potentiodynamic polarization measurements. The circumstances of the corrosion measurements were carefully controlled by the temperature and the pH of the solution with the stirring of the solution during the mea-

Table 2. Mechanical properties of as-cast alloys

Sample	Density ρ (g cm ⁻³)	Ultimate compressive strength UCS (MPa)	Hardness H_{IT} (GPa)	Elastic modulus E_{IT} (GPa)
Mg ₆₆ Zn ₃₀ Ca ₄	2.967	662	3.45	46
Mg ₆₄ Zn ₃₀ Ca ₄ Y ₂	3.020	671	4	69
Mg ₆₂ Zn ₃₀ Ca ₄ Y ₄	3.065	723	3.44	58
Mg ₆₀ Zn ₃₀ Ca ₄ Y ₆	3.066	626	3.22	52

IT – indentation

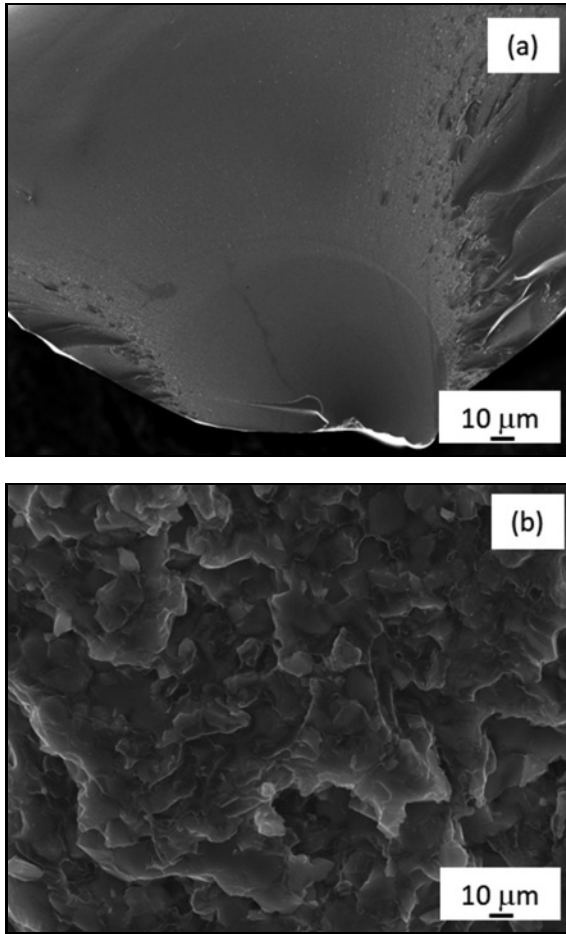
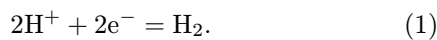


Fig. 4. SEM image of typical brittle fracture observed for all cast alloys (a); SEM image detail of brittle fracture (b).

measurements. Further corrections were applied to the raw data.

For half-reaction:



According to the Nernst equation (Eq. (2)):

$$E_{H^+/H_2} = E^O - \frac{RT}{zF} \ln Q = -\frac{RT}{zF} \ln \left(\frac{p_{H_2}}{[H^+]^2} \right), \quad (2)$$

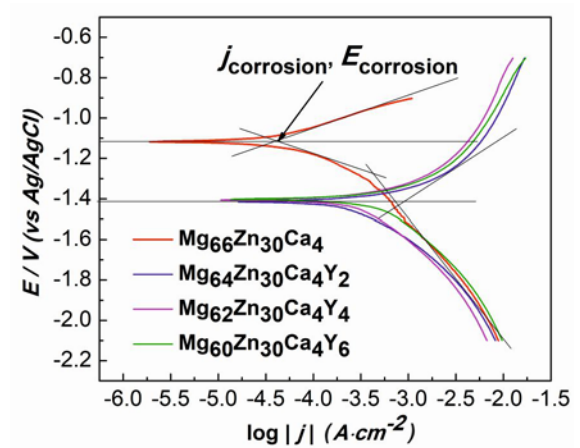


Fig. 5. Tafel plots measured in Hank's solution (pH = 7) at 33°C.

$$E_{H^+/H_2} = -\frac{RT}{zF} \ln \left(\frac{p_{H_2}}{[H^+]^2} \right) = \frac{8.314 \text{ J K}^{-1} \times 298.15 \text{ K}}{2 \times 96485 \text{ J V}^{-1}} \times \ln \left(\frac{1}{[H^+]^2} \right) = 0.012 \text{ V} \times 2 \ln [H^+] = 0.02569 \text{ V} \times 2.303 \log [H^+], \quad (3)$$

$$E_{H^+/H_2} = -0.05916 \text{ V} \times \text{pH}. \quad (4)$$

For the reference system, the corrosion potential of pure Zn was measured, which resulted in -0.99 V as the corrosion potential of pure Zn. The standard potential of Zn (vs H_2 electrode, 0.1 M acid, $\text{pH} = 1$) is -0.79 V . The Hank solution's pH was 6.8. Substitution to the Nernst equation results in -1.139 V at the 6.8 pH value.

The correction of this value with the reference electrode potential (Ag/AgCl, $E = +0.197 \text{ V}$) gives -0.942 V . The error of the measurement was only $\pm 0.05 \text{ V}$ as compared to the literature corrosion potential of pure Zn.

The corrosion rates were calculated (Eq. (5)) based on ASTM G59-97 from the measured Tafel plots (Fig. 5):

Table 3. Corrosion properties of as-cast alloys

Sample	Electrochemical corrosion current density j (A cm ⁻²)	Corrosion rate v (mm year ⁻¹)	Corrosion potential E_{corr}
Mg ₆₆ Zn ₃₀ Ca ₄	4.27×10^{-5}	0.878 ± 0.2	-1.11 ± 0.05
Mg ₆₄ Zn ₃₀ Ca ₄ Y ₂	7.99×10^{-4}	16.7 ± 0.4	-1.41 ± 0.05
Mg ₆₂ Zn ₃₀ Ca ₄ Y ₄	8.69×10^{-4}	18.4 ± 0.4	-1.41 ± 0.05
Mg ₆₀ Zn ₃₀ Ca ₄ Y ₆	6.62×10^{-4}	14.8 ± 0.4	-1.41 ± 0.05

$$CR = 3.27 \times 10^{-3} \frac{j_{\text{corr}}EW}{\rho}, \quad (5)$$

where j_{corr} is the electrochemical corrosion current density (A cm⁻²), EW is the equivalent weight (g), and ρ is the density (g cm⁻³) of the Mg-based materials.

In general, a higher corrosion potential provides better resistance against corrosion. As seen from the Tafel plots, all yttrium-containing samples have lower corrosion potential than the pure Mg₆₆Zn₃₀Ca₄ alloy. From the corrosion rate calculation, it can also be pointed out that the presence of yttrium accelerates the corrosion. However, this property can be advantageous in applications where it is essential that the alloy is only present in the body for a short time and is quickly absorbed by the tissues. The results of corrosion properties of all as-cast alloys calculated from Tafel plots are shown in Table 3.

4. Conclusions

The Mg_{66-x}Zn₃₀Ca₄Y_x ($x = 0, 2, 4, 6$) alloys were prepared by rapid solidification. The microstructure, mechanical tests, and corrosion behavior (by electrochemical test in Hank's solution) were evaluated for all alloys in the as-cast conditions. The following conclusions may be drawn from the present study:

1. After solidification, the Mg₆₆Zn₃₀Ca₄ alloy shows an amorphous structure. The amorphous structure is suppressed with a small amount of Y (2 at.%), and the sharp crystalline peaks are apparent. The alloys with Y addition contain three phases: α -Mg, Mg_{24.25}Y_{4.75}, and an unknown orthorhombic phase similar to the Ga₂Zr phase.

2. The Ultimate Compressive Strength (UCS) and the plastic strain of doped alloys (up to 4 at.%) were significantly improved compared to alloys without Y.

3. Alloys exhibit a typical brittle fracture.

4. All Y microalloying samples have a lower corrosion potential than pure ones. This information could be helpful in the case of possible implant applications for a short period.

Acknowledgements

The authors are grateful to the Slovak Research and Development Agency under contract No. APVV-17-0008 and APVV-20-0068. W. Miženková would like to acknowledge the student grant “06/TUKE/2022”.

References

- [1] H. Kabir, K. Munir, C. Wen, Y. Li, Recent research and progress of biodegradable zinc alloys and composites for biomedical applications: Biomechanical and biocorrosion perspectives, *Bioact. Mater.* 6 (2021) 836–879. <https://doi.org/10.1016/J.BIOACTMAT.2020.09.013>
- [2] M. Kim, S. An, C. Huh, C. Kim, Development of zirconium-based alloys with low elastic modulus for dental implant materials, *Appl. Sci.* 9 (2019) 5291. <https://doi.org/10.3390/APP9245281>
- [3] V. M. S. Muthaiah, S. Indrakumar, S. Suwas, K. Chatterjee, Surface engineering of additively manufactured titanium alloys for enhanced clinical performance of biomedical implants: A review of recent developments, *Bioprinting* 25 (2022) e00180. <https://doi.org/10.1016/J.BPRINT.2021.E00180>
- [4] Z. Morsada, M. M. Hossain, M. T. Islam, M. A. Mobin, S. Saha, Recent progress in biodegradable and bioresorbable materials: From passive implants to active electronics, *Appl. Mater. Today* 25 (2021) 101257. <https://doi.org/10.1016/J.APMT.2021.101257>
- [5] K. Sangeetha, A. V. Jisha Kumari, J. Venkatesan, A. Sukumaran, S. Aisverya, P. N. Sudha, Degradable metallic biomaterials for cardiovascular applications, *Fundam. Biomater. Met.* (2018) 285–298. <https://doi.org/10.1016/B978-0-08-102205-4.00013-1>
- [6] M. M. Zerankeshi, R. Alizadeh, Ag-incorporated biodegradable Mg alloys: A review, *Materialia* (2022) 101445. <https://doi.org/10.1016/J.MTLA.2022.101445>
- [7] J. Song, J. Chen, X. Xiong, X. Peng, D. Chen, F. Pan, Research advances of magnesium and magnesium alloys worldwide in 2021, *J. Magnes. Alloy* 10 (2022) 863–898. <https://doi.org/10.1016/J.JMA.2022.04.001>
- [8] Y. Guo, S. Jia, L. Qiao, Y. Su, R. Gu, G. Li, J. Lian, A multifunctional polypyrrole/zinc oxide composite coating on biodegradable magnesium alloys for orthopedic implants, *Colloids Surfaces B Biointerfaces* 194 (2020) 111186. <https://doi.org/10.1016/J.COLSURFB.2020.111186>

- [9] G. Uppal, A. Thakur, A. Chauhan, S. Bala, Magnesium based implants for functional bone tissue regeneration – A review, *J. Magnes. Alloy* 10 (2022) 356–386. <https://doi.org/10.1016/J.JMA.2021.08.017>
- [10] N. Yang, J. Venezuela, S. Almathami, M. Dargusch, Zinc-nutrient element based alloys for absorbable wound closure devices fabrication: Current status, challenges, and future prospects, *Biomaterials* 280 (2022) 121301. <https://doi.org/10.1016/J.BIOMATERIALS.2021.121301>
- [11] M. Mohammadi Zerankeshi, R. Alizadeh, E. Gerashi, M. Asadollahi, T. G. Langdon, Effects of heat treatment on the corrosion behavior and mechanical properties of biodegradable Mg alloys, *J. Magnes. Alloy* 10 (2022) 1737–1785. <https://doi.org/10.1016/J.JMA.2022.04.010>
- [12] X. Tong, L. Zhu, K. Wang, Z. Shi, S. Huang, Y. Li, J. Ma, C. Wen, J. Lin, Impact of gadolinium on mechanical properties, corrosion resistance, and biocompatibility of Zn-1Mg-*x*Gd alloys for biodegradable bone-implant applications, *Acta Biomater.* 142 (2022) 361–373. <https://doi.org/10.1016/J.ACTBIO.2022.02.015>
- [13] K. Li, Z. Cai, P. Du, T. Xiang, X. Yang, G. Xie, Core-shell Mg₆₆Zn₃₀Ca₄ bulk metallic glasses composites reinforced by Fe with high strength and controllable degradation, *Intermetallics* 138 (2021) 107334. <https://doi.org/10.1016/J.INTERMET.2021.107334>
- [14] K. Saksl, I. Pethes, P. Jóvári, Z. Molčanová, J. Ďurišin, B. Ballóková, L. Temleitner, Š. Michalik, M. Šulíková, K. Šuřová, M. Fejerčák, D. Varcholová, R. Motýl, Atomic structure of the Mg₆₆Zn₃₀Ca₄ metallic glass, *J. Non. Cryst. Solids* 558 (2021) 120660. <https://doi.org/10.1016/J.JNONCRY SOL.2021.120660>
- [15] R. Ahmad, A. M. M. Elasad, M. B. A. Asmael, N. R. Shahizan, Effect of yttrium addition on microstructure and hardness of cast EV31A magnesium alloy, *Key Eng. Mater.* 740 (2017) 81–85. <https://doi.org/10.4028/WWW.SCIENTIFIC.NET/KEM.740.81>
- [16] M. Wang, H. Zhou, L. Wang, Effect of yttrium and cerium addition on microstructure and mechanical properties of AM50 magnesium alloy, *J. Rare Earths* 25 (2007) 233–237. [https://doi.org/10.1016/S1002-0721\(07\)60079-9](https://doi.org/10.1016/S1002-0721(07)60079-9)
- [17] R. Babilas, A. Bajorek, W. Simka, D. Babilas, Study on corrosion behavior of Mg-based bulk metallic glasses in NaCl solution, *Electrochim. Acta* 209 (2016) 632–642. <https://doi.org/10.1016/J.ELECTACTA.2016.05.065>
- [18] W. C. Oliver, G. M. Pharr, An improved technique for determining hardness and elastic modulus using load and displacement sensing indentation experiments, *J. Mater. Res.* 7 (1992) 1564–1583. <https://doi.org/10.1557/JMR.1992.1564>